Dimerization and Charge Order in Hollandite $K_2V_8O_{16}$

A. C. Komarek,[1] M. Isobe,[2] J. Hemberger,[1] D. Meier,[1] T. Lorenz,[1] D. Trots,[3,4] A. Cervellino,[5] M. T. Fernández-Díaz,[6] Y. Ueda,[2] and M. Braden[1]

[1]*II. Physikalisches Institut, Universität zu Köln, Zülpicher Strasse 77, D-50937 Köln, Germany*
[2]*Institute for Solid State Physics, University of Tokyo, Kashiwa, Chiba 277-8581, Japan*
[3]*Darmstadt University of Technology, Institute for Material Science, Petersenstrasse 23, D-64287 Darmstadt*
[4]*Hasylab/DESY Notkestrasse 85, D-22607, Hamburg, Germany*
[5]*Laboratory for Neutron Scattering, PSI Villigen and ETH Zurich CH-5232 Villigen PSI, Switzerland*
[6]*Institut Laue Langevin, BP156X, 38042 Grenoble Cedex, France*

(Received 14 December 2010; published 5 July 2011)

The metal-insulator transition occurring in hollandite $K_2V_8O_{16}$ has been studied by means of neutron and x-ray diffraction as well as by thermodynamic and electron-spin resonance measurements. The complete analysis of the crystal structure in the distorted phase allows us to identify dimerization as the main distortion element in insulating $K_2V_8O_{16}$. At low-temperature, half of the V chains are dimerized perfectly explaining the suppression of magnetic susceptibility due to the formation of spin singlets. The dimerization is accompanied by the segregation of charges into chains.

DOI: 10.1103/PhysRevLett.107.027201 PACS numbers: 75.47.Lx, 61.05.C−, 72.80.Ga

Vanadium oxides exhibit a variety of fascinating properties. V_2O_3 and VO_2 [1] are key compounds for the general understanding of metal-insulator (MI) transitions. β-$Na_{0.33}V_2O_5$, β-$Ag_{0.33}V_2O_5$, and β'-$Cu_{0.65}V_2O_5$ [2–4] exhibit superconductivity at high pressure, most likely related with charge ordering instabilities at ambient pressure. Originally, hollandite was a manganese-oxide mineral [5], but this name now refers to compounds with the general formula $A_xM_8O_{16}$ ($x \leq 2$) [6]. $K_2Cr_8O_{16}$ is a rare case of a ferromagnetic insulator driven through orbital ordering [7–10], and $K_2V_8O_{16}$ is a mixed-valent vanadium oxide which attracts strong experimental and theoretical interest [11–15] due to its poorly understood MI transition. At room temperature, $K_2V_8O_{16}$ exhibits a tetragonal structure, space group $I4/m$, that is built of double chains of edge-sharing VO_6 octahedrons, see Fig. 1. The structure of $K_2V_8O_{16}$ is closely related with the rutile structure of VO_2, just the rutile single chains are replaced by double chains and the K introduces an electronic doping with an average V valence of +3.75. $K_2V_8O_{16}$ exhibits a two-step MI transition [11] in which the electronic transition is accompanied by a structural phase transition, and, most interestingly, by a drop in the magnetic susceptibility. In spite of serious efforts the character of the insulating phase in $K_2V_8O_{16}$ has not been established and different models are discussed for the charge, orbital, and spin order [11–15]. Therefore, we have performed comprehensive diffraction experiments to determine the structural distortion of $K_2V_8O_{16}$ in its insulating phase.

Within the polycrystalline samples synthesized using a high-pressure technique [11] it was possible to find single-crystalline grains large enough to collect comprehensive sets of Bragg intensities on a *Bruker X8 Apex* CCD diffractometer (Mo-K_α radiation). Data sets have been recorded at ten temperatures between 300 and 100 K, each of them with 95% completeness up to $\sin(\theta)/\lambda \sim 0.95$. Structural models have been refined using the JANA program package [16] taking twinning into account. In addition we performed powder-diffraction measurements at the synchrotron-radiation beam line B2 at Hasylab/DESY and at the two neutron beam lines DMC (Paul Scherrer Institute) and D2B (Institut Laue Langevin). Electron-Spin Resonance (ESR) studies were carried out with a Bruker *ELEXSYS E500* CW spectrometer.

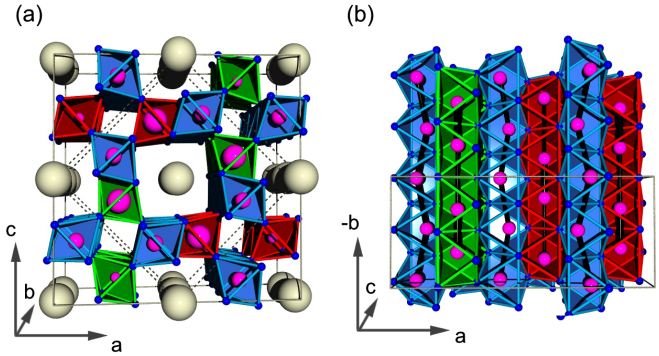

FIG. 1 (color online). The low-temperature monoclinic structure of $K_2V_8O_{16}$ (a). The high-temperature tetragonal cell ($10 \times 10 \times 2.9$ Å^3) and the monoclinic cell are indicated by dashed and gray lines, respectively (note that c_{tet} axis becomes b_{mono}). Blue (small): oxygen, gray (large): potassium, magenta (other): vanadium; green (light), red (dark), or blue (other) octahedra contain dimerized V^{3+}, dimerized V^{4+}, or nondimerized V^{4+} in zigzag chains. Large (small) spheres denote V ions dimerized with a V ion in the next (in the same) unit cell in b_{mono} direction. (b) Side view of two unit cells. All K^+ ions have been omitted.

Figure 2(a) shows the intensity profiles of three different reflections taken from synchrotron-radiation powder-diffraction patterns. The lattice parameters derived from Rietveld refinements are plotted in Figs. 2(b)–2(d). The temperature dependencies of the resistivity and that of the specific heat, see Fig. 3, indicate two phase transitions appearing at $T_1 \sim 150$ K and $T_2 \sim 170$ K upon cooling in agreement with previous reports. The magnetic susceptibility presents hysteretic behavior in a broad temperature range between T_1 and T_2, see Fig. 3(b). Upon cooling, the magnetic susceptibility starts to deviate from its high-temperature behavior already at T_2 and exhibits a sharp drop by about 50% of its value at T_1. The synchrotron measurements confirm the phase transition from a tetragonal phase to a monoclinic phase in the temperature range between T_1 and T_2 as reported previously [11]. The concomitant broadening or splitting of both the $(110)_{\text{tet}}$ and of the $(200)_{\text{tet}}$ reflections excludes an orthorhombic symmetry in the low-temperature phase. The $(211)_{\text{tet}}$ peak at larger scattering angle clearly indicates phase coexistence between T_1 and T_2, but below T_1 only a single phase is visible [17]. X-ray diffraction measurements on a single-crystalline sphere with 100 μm diameter reveal a large number of strong superstructure reflections, see the inset of Fig. 3(c), which are of the type $(\frac{1}{2}, \frac{1}{2}, \frac{1}{2})_{\text{tetra}}$. For one of them, the temperature dependence is shown revealing again hysteretic behavior. Although there is already weak intensity for $T_1 < T < T_2$, the main intensity increase occurs at the lower transition perfectly reflecting the strong anomalies in magnetic susceptibility and in specific heat. The increase in resistivity occurs in two steps, see Fig. 3(e),

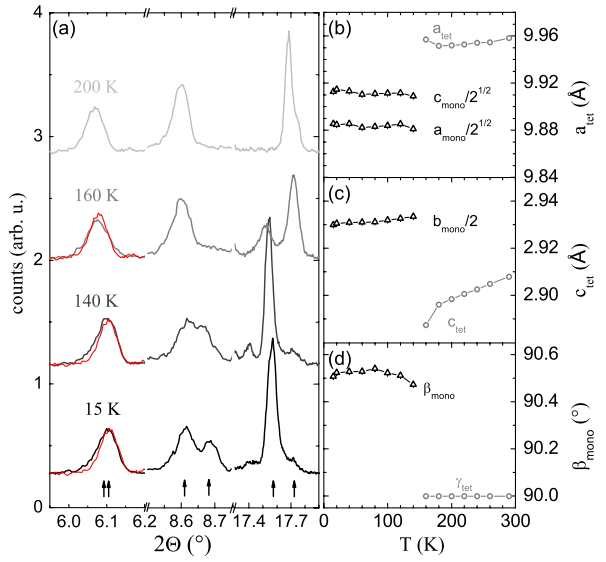

FIG. 2 (color online). (a) Synchrotron powder x-ray diffraction patterns of $K_2V_8O_{16}$. The first reflection shown is a $(2\,0\,0)_{\text{mono}}$ or $(0\,0\,2)_{\text{mono}}$ reflection. The 200 K-data [red (light)] are superposed with the data at low temperatures to illustrate the peak broadening. The second peak is a $(\pm 2\,0\,2)_{\text{mono}}$ peak and the third $(\pm 3\,2\,1)_{\text{mono}}$ reflection indicates phase coexistence near 160 K. (b)–(d) Lattice parameters.

but the phase coexistence and the related percolation effects prevent a quantitative analysis and most likely cause the minor shifts in the temperatures of the observed anomalies.

All superstructure reflections can be indexed by a monoclinic $\sqrt{2}a \times \sqrt{2}a \times 2c$ cell which is rotated by 45°, see Fig. 1. A nonrotated $2a \times 2a \times 2c$ F-centered orthorhombic cell can be excluded due to symmetry conditions and as it is not able to explain the peak broadening of the first peak shown in Fig. 2(a). Also the monoclinic lattice, doubling the tetragonal axis and only one of the in-plane constants, can be excluded, as this configuration does not yield the observed superstructure reflections even when taking twinning into account. There are only a few maximum isotropy subgroups consistent with the observed loss of translation symmetry: $I2/m$, $I2/c$, and $I2$. The distorted structure can be refined without any constraints in the space groups $I2/m$ and $I2/c$ yielding much better reliability (R) values for the $I2/m$ model. The unweighted and the weighted R values for the $I2/m$ model amount to 3% and 5%, respectively, whereas the refinements in $I2/c$ yield 11% and 21%, respectively. The refinement of the crystal structure based on the lower symmetry $I2$ implies 30 atoms in

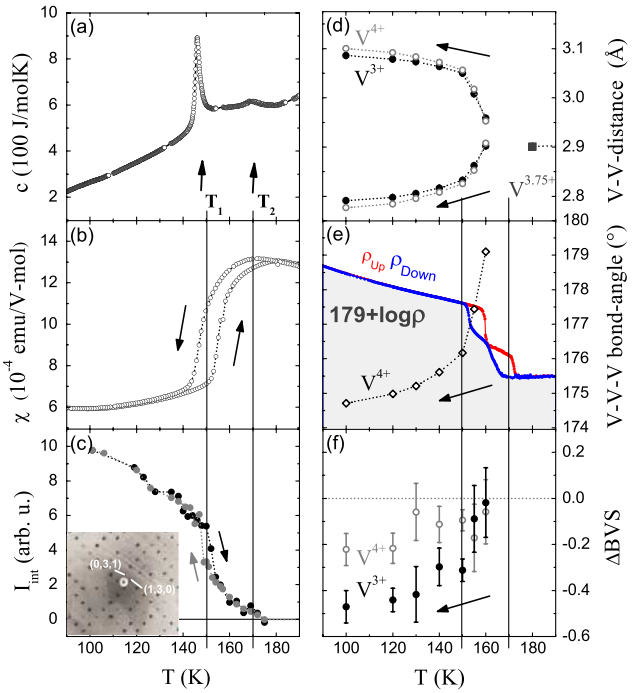

FIG. 3 (color online). Specific heat (a) and magnetic susceptibility (b) of $K_2V_8O_{16}$. (c)–(f) Results of single-crystal x-ray diffraction measurements. (c) Intensity of the $(0.51.51.5)_{\text{tet}} = (2\,3\,1)_{\text{mono}}$ superstructure reflection normalized to the fundamental $(0\,2\,2)_{\text{tet}}$ reflection. The inset shows superstructure reflections within a $(hk1.5)_{\text{tet}} = (h3l)_{\text{mono}}$ plane. (d) The V-V bond-lengths indicating the dimerization; black: V1-V1, gray: V4-V4. (e) The V-V-V bond-angle, i.e., the angle of the zigzag chains; for comparison we also show the resistivity in $\mu\Omega$ cm as $179 + \log(\rho)$ (f) Difference in the BVS of the dimerized V1 and V4 ions compared to the average BVS of the V ions within the zigzag chains (all very close to 4 +).

the asymmetric unit preventing the free refinement of all parameters to converge. The refinements in space group $I2$ do not yield a significant improvement in the R values; this further symmetry reduction is, therefore, not supported by the intensity data. There are several thousand superstructure-reflection intensities entering the refinements with the strongest ones possessing about 0.75% of the intensity of the strongest fundamental reflections. Therefore, the deduced structural model given in Fig. 1 and in Table I is unambiguous.

In the high-temperature phase there are mirror planes at $z = 0$ and at $z = 0.5$ containing all V atoms. The symmetry reduction from $I4/m$ to $I2/m$ in the larger unit cell entails the suppression of every second mirror plane. Consequently, in a double chain all the V atoms of one chain still lie on a mirror plane, whereas the V atoms of the neighbor chain lie between two mirror planes. The latter configuration gives rise to dimerization associated with an alternating V displacement along the monoclinic b axis that are remarkably strong, of the order of tenths of an Å, see Fig. 3(d). In comparison the modulations of the V-O distances reflecting charge ordering are much weaker. There are two symmetrically independent dimerized chains, each of them containing only a single independent V site, V1 and V4. Each of the double chains contains one dimerized and one nondimerized chain. In the nondimerized chains neighboring a dimer chain there are two independent V sites, as one site is close to a dimer and another one lies between two dimers. As there are two types of nondimerized chains, there are four crystallographically independent V sites in the nondimerized chains. These V atoms exhibit displacements perpendicular to the chains whose direction alternates along the chain causing a zigzag arrangement. The V atoms in the nondimerized chains move away from the dimers and towards the space in between two dimers, see the double chain in the middle of Fig. 1(b), so that the corresponding V-V distances vary very little along the double chains. This behavior strongly supports the plausibility of the structural solution. The temperature dependence of the V-V distances within the dimerized chains and that of the V-V-V bond angles (in c_{tet} direction) in the nondimerized chains are shown in Figs. 3(d) and 3(e), respectively; these distortions of the $I4/m$ structure, which both are directly coupled with the dimerization, are remarkably strong.

TABLE I. Results of single-crystal x-ray diffraction measurements of $K_2V_8O_{16}$ at 100 K.

a: 13.9773(9) Å, b: 5.8773(4) Å, c: 13.9773(9) Å, β: 89.481°				
	x	y	z	U_{iso}(Å^2)
K1	0	0.25014(6)	0	0.00435(14)
K2	0.5	0.5	0	0.0344(5)
K3	0.5	0	0	0.0347(5)
V1	0.24290(10)	0.26262(6)	0.09062(10)	0.00592(13)
V2	0.73881(9)	0.5	0.09262(9)	0.00560(15)
V3	0.74587(10)	0	0.08644(9)	0.00544(14)
V4	0.09103(10)	0.26386(6)	−0.24409(11)	0.00618(13)
V5	0.09519(9)	0.5	−0.73930(10)	0.00465(14)
V6	0.08842(10)	0	−0.74616(11)	0.00685(15)
O1	0.1774(6)	0	0.0196(7)	0.0067(10)
O2	0.6755(6)	0.25173(14)	0.0214(7)	0.0049(9)
O3	0.1751(6)	0.5	0.0156(7)	0.0060(9)
O4	0.3144(5)	0	0.1499(5)	0.0089(12)
O5	0.8142(4)	0.24852(14)	0.1507(4)	0.0034(9)
O6	0.3176(5)	0.5	0.1514(5)	0.0085(12)
O7	0.0247(5)	0	−0.1791(4)	0.0023(7)
O8	0.0179(5)	0.25143(15)	−0.6757(5)	0.0072(8)
O9	0.0225(5)	0.5	−0.1771(5)	0.0033(7)
O10	0.1501(6)	0	−0.3162(6)	0.0082(9)
O11	0.1461(5)	0.24978(13)	−0.8148(4)	0.0032(7)
O12	0.1507(5)	0.5	−0.3199(5)	0.0073(9)
Refl. 31852	Av. refl. 4861	Redund. 6.55	$2\Theta_{\mathrm{max}}$ 92.5°	
R_{int} 2.54%	R 3.06%	R_w 5.14%	GoF 2.58	

The dimerization in half of the chains forms the main element of the structural distortion in $K_2V_8O_{16}$ at low temperatures. There is a strong impact on the magnetism as V spins in the dimerized chains become coupled into singlets perfectly explaining the drop in magnetic susceptibility by roughly 50%, see Fig. 3(b). Furthermore, the V spins in the nondimerized chains become effectively isolated as each magnetic zigzag chain is surrounded by dimerized chains. The V spins in the zigzag chains thus form separated spin-$\frac{1}{2}$ Heisenberg chains rendering studies at very low temperature highly desirable.

The precise crystal structure allows for analyzing the charge ordering with the bond-valence sum (BVS) formalism [18]. In the room-temperature phase we find a BVS of 3.86(1). At 100 K all V sites in the zigzag nondimerized chains show a BVS close to V^{4+}, but one half of the dimerized chains (V1 site) exhibits a BVS which is roughly 0.5 below the value of 4. The value for the other dimerized vanadium chain is again more close to 4. Therefore, we may conclude that charge ordering occurs in the low-temperature insulating phase of $K_2V_8O_{16}$. Most interestingly, the excess electrons segregate into single chains, which furthermore are dimerized. One fourth of the V ions is formed by the V1 site in perfect agreement with the quarter doping in $K_2V_8O_{16}$. The segregation of charges into dimerized chains disagrees with the simple picture of a Wigner lattice; however, it resembles the stripe ordering in layered transition-metal oxides. The fact that the modulation of the bond-valence sum is smaller than the expected integer charge modulation reflects the behavior observed in many $3d$-transition-metal oxides; the modulation by ~0.5 electron charges in $K_2V_8O_{16}$ is among the larger ones.

The hysteretic transitions and the phase coexistence for $T_1 < T < T_2$ hinder the analysis of the temperature dependence of the MI transition. In the single-crystal experiment we cannot separate the coexisting phases. Therefore, the obtained distortion represents the average distortion. The first resistivity increase occurs at T_2 when

only parts of the sample start to transform, but the lower transition causes a comparable increase in resistivity on the logarithmic scale. As also the structural distortions metered by the superstructure-reflection intensities increase at both transitions, the driving element of the metal-insulator transition cannot be clearly identified at present.

The structural distortion in $K_2V_8O_{16}$ strongly resembles that in the monoclinic M2 phase of VO_2 [19–21] where also only a part of the chains dimerize. It appears likely that the double-chain structure in $K_2V_8O_{16}$ prevents complete dimerization. A very similar behavior is also observed in V_4O_7 which exhibits charge ordering at low temperature with dimerized V^{3+} chains and dimerized V^{4+} chains [22].

Powder neutron-diffraction patterns measured at the high-flux DMC diffractometer yield no indication for antiferromagnetic ordering in spite of their high statistics ($\lambda = 2.45$ Å). Additional neutron patterns were taken at the high-resolution diffractometer D2B ($\lambda = 1.5944$ Å). The model obtained by single-crystal x-ray diffraction perfectly describes the D2B data excluding that the model overlooks a significant structural distortion.

The ESR parameters are obtained by fitting the spectra with a Dyson line [23], see Figs. 4(a)–4(d). The linewidth ΔH and the g factor, which is close to $g = 2$, are both nearly temperature independent and do not show pronounced anomalies close to T_{MI}. This points towards the absence of antiferromagnetic order and, thus, corroborates our dimerization scenario. The intensity of the ESR line is displayed in Fig. 4(c). In contrast to the macroscopic susceptibility the line intensity shows an increase on cooling below the MI transition. This apparent contradiction can be explained by the strong change of the conductivity at the MI transition [11]. The dispersion to absorption (D/A) ratio reflects the skin effect induced dispersion superposing the ESR absorption that leads to asymmetric deviations from the usual Lorentzian line shape, compare Fig. 4(b). The increase of the skin depth (for $\nu = 9.36$ GHz) causes an enhancement of the ESR signal in the insulating regime, overcompensating the effect of spin dimerization sensed by the bulk susceptibility. On the other hand the strong ESR signal at low temperatures clearly indicates that not all spins dimerize, in accordance with our model.

In conclusion, the comprehensive crystal structure determination in the low-temperature phase of $K_2V_8O_{16}$ closes the controversy about the character of this insulating phase with peculiar magnetic properties. Dimerization in half of the chains forms the main element of the structural distortion at low temperature; in addition there is a zigzag displacement perpendicular to the chains appearing in the neighboring nondimerized chains. The excess electrons segregate into dimerized chains. This structural distortion is associated with a major change in the magnetic character of $K_2V_8O_{16}$. Spins in the dimerized chains become coupled into singlets rendering the dimer chains nonmagnetic in perfect agreement with the roughly 50% drop in magnetic susceptibility. Furthermore, the remaining magnetic sites are confined into the nondimerized chains, which are well isolated from each other, so that $K_2V_8O_{16}$ becomes a good realization of spin $\frac{1}{2}$ Heisenberg chains.

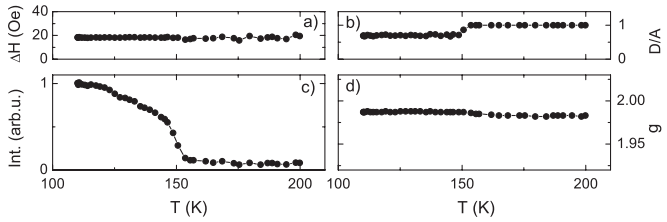

FIG. 4. Parameters of the ESR line as a function of temperature as measured on heating: (a) linewidth, (b) D/A ratio, (c) intensity, and (d) g factor.

This work was supported by the Deutsche Forschungsgemeinschaft through SFB 608 and by the Japan Society for the Promotion of Science through Grant-in-Aid for Scientific Research (No. 18104008). We thank D. Khomskii for stimulating discussions.

[1] M. Foëx, Compte Rendu **223**, 1126 (1946); **227**, 193 (1948); F. J. Morin, Phys. Rev. Lett. **3**, 34 (1959).
[2] T. Yamauchi Y. Ueda, and N. Môri, Phys. Rev. Lett. **89**, 057002 (2002).
[3] T. Yamauchi *et al.*, Solid State Sci. **7**, 874 (2005).
[4] Y. Ueda *et al.*, J. Phys. Chem. Solids **63**, 951 (2002).
[5] A. Byström and A. M. Byström, Acta Crystallogr. **3**, 146 (1950).
[6] S. Ishiwata *et al.*, J. Phys. Condens. Matter **18**, 3745 (2006).
[7] K. Hasegawa *et al.*, Phys. Rev. Lett. **103**, 146403 (2009).
[8] P. Mahadevan *et al.*, Phys. Rev. Lett. **104**, 256401 (2010).
[9] M. Sakamaki, T. Konishi, and Y. Ohta, Phys. Rev. B **80**, 024416 (2009).
[10] M. Sakamaki, T. Konishi, and Y. Ohta, Phys. Rev. B **82**, 099903(E) (2010).
[11] M. Isobe *et al.*, J. Phys. Soc. Jpn. **75**, 073801 (2006).
[12] M. Isobe *et al.*, J. Phys. Soc. Jpn. **78**, 114713 (2009).
[13] M. Isobe *et al.*, J. Magn. Magn. Mater. **310**, 888 (2007).
[14] S. Horiuchi and Y. Ohta, J. Phys. Chem. Solids **69**, 3379 (2008).
[15] S. Horiuchi, T. Shirakawa, and Y. Ohta, Phys. Rev. B **77**, 155120 (2008).
[16] V. Petricek, M. Dusek, and L. Palatinus, *Jana2006 The Crystallographic Computing System* (Institute of Physics, Praha, 2006).
[17] Note that there is some minor yet unidentified impurity phase visible (of the order of 5%).
[18] I. D. Brown and D. Altermatt, Acta Crystallogr. Sect. B **41**, 244 (1985).
[19] J. P. Pouget *et al.*, Phys. Rev. B **10**, 1801 (1974).
[20] T. M. Rice, H. Launois, and J. P. Pouget, Phys. Rev. Lett. **73**, 3042 (1994).
[21] V. Eyert, Ann. Phys. (N.Y.) **11**, 650 (2002).
[22] J.-L. Hodeau and M. Marezio, J. Solid State Chem. **23**, 253 (1978).
[23] S. E. Barnes, Adv. Phys. **30**, 801 (1981).